ISPRS Journal of Photogrammetry and Remote Sensing 205 (2023) 135–146

Contents lists available at ScienceDirect

ISPRS Journal of Photogrammetry and Remote Sensing

journal homepage: www.elsevier.com/locate/isprsjprs

Multi-year hyperspectral remote sensing of a comprehensive set of crop foliar nutrients in cranberries

Nanfeng Liu [a,*], Erin Wagner Hokanson [b], Nicole Hansen [c], Philip A. Townsend [d]

[a] Carbon-Water Research Station in Karst Regions of Northern, Guangdong Provincial Key Laboratory of Urbanization and Geo-simulation, School of Geography and Planning, Sun Yat-Sen University, Guangzhou 510275, China
[b] Space Science and Engineering Center, University of Wisconsin-Madison, Madison, WI 53715, USA
[c] Cranberry Creek Cranberries, Inc, Necedah, WI 54646, USA
[d] Department of Forest and Wildlife Ecology, University of Wisconsin-Madison, Madison, WI 53705, USA

ARTICLE INFO

Keywords:
Foliar nutrients
Hyperspectral remote sensing
Machine learning
Physical basis

ABSTRACT

Hyperspectral remote sensing has emerged as an efficient tool to quantify the spatial and temporal variations in crop foliar nutrients, thus reducing the burden on in-situ tissue sampling and traditional chemical assays. However, the physical mechanism of hyperspectral remote sensing of foliar nutrients is under-explored, especially for those lacking absorption features. Using four-year data collected from a cranberry farm, we demonstrate the capacity of leaf and imaging spectroscopy to quantify a comprehensive set of crop foliar nutrients, including seven macronutrients (N, P, K, Mg, Ca, S, Na) and five micronutrients (Fe, Mn, B, Cu, Zn). Specifically, we: 1) compared the performance of four data-driven approaches to estimate foliar nutrients at both leaf and canopy scales, including partial least square regression (PLSR), support vector regression (SVR), Gaussian process regression (GPR) and random forest regression (RFR); and 2) explored the physical basis of hyperspectral remote sensing of foliar nutrients. Our results showed that: 1) at leaf scales linear approaches PLSR and SVR performed best for nine nutrients (P, Mg, Ca, S, Na, Fe, B, Cu and Zn), whereas nonlinear approaches GPR and RFR performed best only for three nutrients (N, K and Mn); 2) at canopy scales no data-driven approach significantly outperformed others; 3) the best modelling accuracy varied with foliar nutrients (leaf scales: R^2 from 0.30 to 0.93 and RRMSE from 9 to 51%; canopy scales: R^2 from 0.15 to 0.81 and RRMSE from 7 to 37%). The physical basis of hyperspectral remote sensing of foliar nutrients was mainly attributed to their strong correlations with leaf compounds that have apparent absorption features. More specifically, at leaf scales the correlation between foliar nutrients and LMA (leaf mass per area) was leveraged by models to predict foliar nutrients from leaf spectra; at canopy scales the correlation of foliar nutrients with leaf chlorophyll and canopy LAI (Leaf area index) was leveraged by models to predict foliar nutrients from canopy spectra. This study revealed the importance of trait correlations in predicting foliar nutrients, and improved our understanding of the physical mechanisms in hyperspectral remotes sensing of foliar nutrients.

1. Introduction

The American cranberry (*Vaccinium macrocarpon* Ait.) is a short, woody and evergreen perennial plant that is grown as a commercial crop in North America. Commercial cranberries are typically grown in marshes or bogs and their crop quality and production are greatly impacted by nutrient management, including the timing, source and dosage of fertilizer applications (Davenport, 1996; Jamaly et al., 2021; Parent et al., 2021). For example, a deficiency in nitrogen supply decreases the density and yield of berries (Jamaly et al., 2021; Roper, 2006), whereas an overapplication of nitrogen leads to plant crowding, impedes pollinators and decreases yield (De Moranville and Ghantous, 2018). Phosphorus is important for root development and plant metabolism. However, excess phosphorus may result in the eutrophication of surface water (De Moranville, 2014; Parent and Marchand, 2006). Some micronutrients such as aluminum, zinc and copper become toxic when oversupplied (Roper, 2006). Because cranberries are grown in acidic soils, management of aluminum and iron, as well as tracking of acid-sensitive cations such as calcium, is critical to maintaining plant health and productivity (De Moranville and Ghantous, 2018).

* Corresponding author.
E-mail address: liunf3@mail.sysu.edu.cn (N. Liu).

https://doi.org/10.1016/j.isprsjprs.2023.10.003
Received 11 June 2023; Received in revised form 3 September 2023; Accepted 7 October 2023
Available online 12 October 2023

Plant tissue analysis is conventionally used for assessing the nutrient status of cranberries (Harbut, 2011). In practice, growers annually collect leaf samples from a subset of cranberry beds and send them to a lab for chemical analysis. Lab analysis typically reports the concentrations of 12 foliar nutrients, including seven macronutrients (nitrogen, phosphorus, potassium, magnesium, calcium, sulfur, sodium) and five micronutrients (iron, manganese, boron, copper and zinc). Tissue analysis usually occurs between mid-August and mid-September, a period when the cranberry growth in the current year is finished and the nutrient concentrations are relatively stable (Davenport et al., 1995), thereby informing nutrient management practices for the next year.

Tissue analysis cannot provide spatially complete information about the nutrient status of cranberries. It is time consuming, costly and labor intensive. Therefore, tissue samples are often taken at few and widely separated cranberry beds. In our study site, the growers were able to sample only 30% of the cranberry beds for tissue analysis, with the actual tissues collected from a small number of plants in each of their approximately 50 × 350 m beds. With spatially limited samples, it is difficult for growers to make management decisions for those cranberry beds not receiving tissue analysis, and even for unsampled areas of the beds for which sample collections were made.

Reflectance spectroscopy (i.e., hyperspectral remote sensing) at the leaf level and from imagery has emerged as an efficient tool to quantify and map foliar biochemicals (Abdel-Rahman et al., 2017; Abukmeil et al., 2022; Asner et al., 2015; Axelsson et al., 2013; Bian et al., 2013; Chen et al., 2022; Cheng et al., 2014; Gao et al., 2019, 2020; Gara et al., 2022; García-Haro et al., 2020; Li et al., 2017; Pullanagari et al., 2021, 2016; Singh et al., 2022; Van Cleemput et al., 2018; Verrelst et al., 2016, 2021; Wang et al., 2020, 2019; Watt et al., 2020, 2019; Xu et al., 2022; Zhang et al., 2013), thus reducing the burden on in-situ tissue sampling and traditional chemical assays (Asner et al., 2015). Chemometric methods build quantitative linkages between in-situ measured foliar biochemicals and the narrowband spectra acquired from spectroscopy using various statistical models, among which partial least squared regression (PLSR), support vector regression (SVR), Gaussian process regression (GPR) and random forest regression (RFR) are the most used (Verrelst et al., 2015). PLSR linearly transforms spectral reflectance to a small set of orthogonal features (called “latent factors”), and then linearly regresses these features against biochemicals (Chlus and Townsend, 2022; Liu et al., 2021). SVR nonlinearly transforms spectral reflectance to a feature space with a higher dimensionality, and subsequently builds a linear relationship between the transformed features and biochemicals (Axelsson et al., 2013; Pullanagari et al., 2016). GPR assumes all data points to be sampled from a joint multivariate normal distribution, and infers biochemicals from spectral reflectance using the Bayesian rule (Verrelst et al., 2016; Wang et al., 2019). RFR utilizes the “bagging” approach to construct a large number of decision trees, within which various thresholds are applied to spectral reflectance to estimate biochemicals (Feilhauer et al., 2015; Pullanagari et al., 2016).

Numerous studies have compared these approaches (Abdel-Rahman et al., 2017; Axelsson et al., 2013; Feilhauer et al., 2015; Gökkaya et al., 2015; Pullanagari et al., 2016; Singh et al., 2022; Wang et al., 2019). Feilhauer et al. (2015) examined the performance of PLSR, SVR and RFR in predicting leaf chlorophyll, dry matter and water content from leaf reflectance. They found that: 1) PLSR and SVR achieved similar prediction accuracy whereas RFR produced the poorest accuracy; 2) The important spectral bands identified by the three methods were consistent with the reported absorption features of leaf biochemicals. Pullanagari et al. (2016) compared the ability of PLSR, kernel PLSR, SVR and RFR to predict 11 pasture foliar nutrients from canopy reflectance, and found that RFR produced a better prediction for the majority of nutrients than other methods. Wang et al. (2019) evaluated the ability of PLSR and GPR to model 15 grassland biochemicals from canopy reflectance. They found that the two methods performed comparably with respect to both prediction accuracy, uncertainties and the selection of informative bands. Our survey of the literature suggests that there is no best data-driven approach for foliar nutrient prediction using hyperspectral data, and that model selection may depend on the taxa being characterized and the specific chemicals of interest. As such, our approach is to implement multiple model formulations, with the selection of the actual model for mapping based on performance against withheld data or, alternatively, using an ensemble approach (Feilhauer et al., 2015).

The successful retrieval of leaf biochemicals from hyperspectral signals is often attributed to their strong absorption features. Examples can be found from leaf chlorophyll, dry matters and water that have strong absorption features within 400–2500 nm (Feilhauer et al., 2015; Verrelst et al., 2015). However, most foliar nutrients except for nitrogen do not have strong absorption features related to molecular bonds with C, H, N or O within 400–2500 nm (Pandey et al., 2017; Singh et al., 2022). This is mainly because these elements exist as ions in plants or as minor constituents of much larger carbon-based molecules. Previous studies have generally attributed the success of foliar nutrient remote sensing to the correlation between foliar nutrients and those leaf compounds that do have spectral features (Chlus and Townsend, 2022; Mutanga et al., 2005; Pandey et al., 2017; Pullanagari et al., 2016). Since foliar nutrients correlate with some leaf compounds and these compounds can affect reflectance by strong absorptions, an indirect linkage exists between foliar nutrients and reflectance, allowing us to statistically relate foliar nutrients to reflectance. However, the physical basis of the foliar nutrient models is still under-explored.

Our main objective of this research is to test the capacity of both leaf and imaging spectroscopy to quantify the foliar nutrients in cranberries. In application, we: 1) evaluate the performance of leaf and imaging spectroscopy in estimating foliar nutrients; and 2) explore the physical basis of hyperspectral remote sensing of foliar nutrients at both leaf and canopy scales.

2. Study site and data collection

2.1. Study site

Our study site includes 210 50 × 350 m commercial cranberry beds in Juneau County, Wisconsin, USA (Fig. 1). Wisconsin is the leading cranberry producing state in the US, accounting for half of US cranberry production and over 25% of global production (United States Department of Agriculture, 2022). The beds in our imagery include twelve cranberry cultivars: “Ben Lear”, “Bergman”, “Crimson Queen”, “Demoranville”, “Grygleski GHI”, “HyRED”, “Le Munyon”, “Mullia Queen”, “Ruby Star”, “Stevens”, “Sundance” and “Pilgrim” (Fajardo et al., 2013; Roper, 2008). The growing season of cranberries runs from mid-May to early September (DeMoranville, 1992; Hagidimitriou and Roper, 1995). Bud growth initiates in mid-May with shoot elongation and leaf expansion. Flowering begins in late June and continues for 3–4 weeks into July. Floral induction occurs soon after flowering and fruit matures in 60–120 days, depending on cultivars and weather conditions. Harvest starts in late September and continues for 2–3 weeks into October.

2.2. Data collection

Fieldwork was conducted during the growing seasons of 2018–2021, and included tissue samples for chemistry analyses, dry leaf spectra from an ASD spectroradiometer and canopy spectra from two Hyspex imaging spectrometers (Table 1). Foliar nutrients and dry leaf spectra were measured for cranberry uprights, the vertical branches originating from vines and terminating with a vegetative bud. Canopy spectra were collected for cranberry beds using a boresighted Hyspex VNIR-SWIR imaging system.

a) Dry leaf spectra

Dry leaf spectra were measured from 410 cranberry uprights

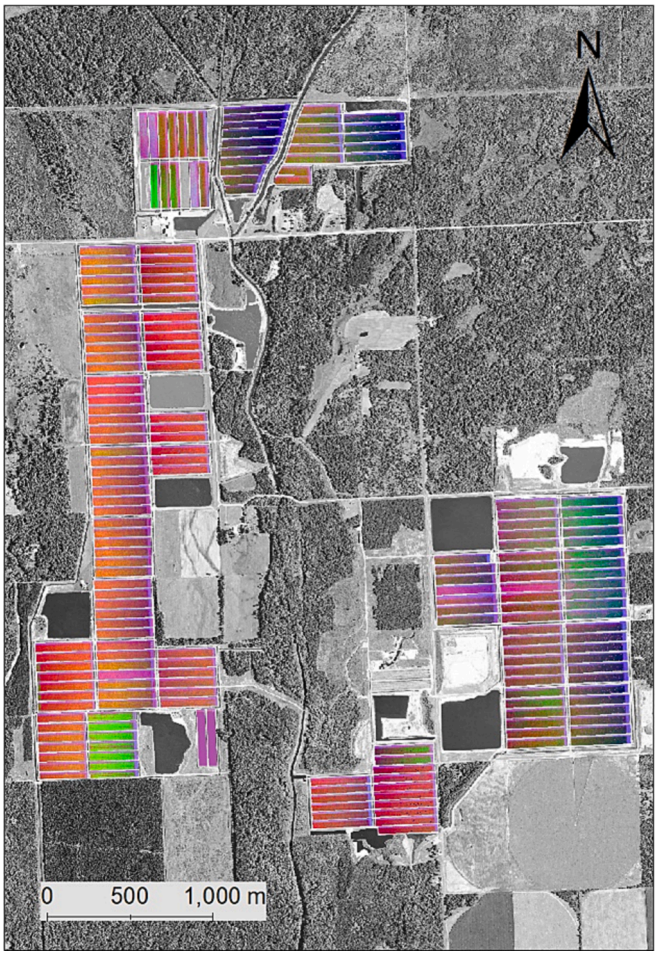

Fig. 1. Cranberry beds from Juneau County, Wisconsin. A NAIP image (National Agriculture Imagery Program, downloaded from: https://relief.ersc.wisc.edu/wisconsinview/form.php) is used as the base map in the black-white color. A minimum noise fraction (MNF) transform is performed to the Hyspex spectra of cranberry areas to show the spectral variations among cranberry beds.

sampled on four dates ("Dry leaf spectra" in Table 1). The sampling dates 2018–07-03, 2019–06-26 and 2021–06-22 were chosen to assess the leaf characteristics in the early growing season when fruits began to form, and 2019–09-04 was to assess the leaf characteristics in the late growing season when fruit matured. Each cranberry bed was evenly split into halves and ten cranberry uprights were randomly collected within each half bed to double the sample size.

We adopted the procedure to measure dry leaf spectra reported by (Serbin et al., 2014; Wang et al., 2020). Leaf samples were oven-dried at 65 °C for at least 48 h. Then, dry leaves were ground to pass through a 20-mesh sleeve (0.84 mm) and weighed by a digital scale (precision: 0.0001 g). Finally, ~350 mg dried and ground leaf material was poured into a black-painted cup, from which the reflectance of leaf material was measured using an ASD spectrometer and a contact probe (Malvern Panalytical Inc., Westborough, Massachusetts, USA; see Serbin et al. 2014). Spectral measurements were made for old and new growth leaves separately. This was not done for the late season sampling date 2019–09-04, at which time old and new foliage were visually indistinguishable.

b) Foliar nutrients

A total of 269 cranberry upright samples were analyzed for 12 foliar nutrients, including seven macronutrients (nitrogen (N), phosphorus (P), potassium (K), magnesium (Mg), calcium (Ca), sulfur (S), sodium (Na)) and five micronutrients (iron (Fe), manganese (Mn), boron (B), copper (Cu) and zinc (Zn)) ("Foliar nutrients" in Table 1). The samples analyzed at Brookside Laboratories (New Bremen, Ohio, USA) were collected by the University of Wisconsin team (sample size: 130), while the samples analyzed at Midwest Laboratories (Omaha, Nebraska, USA) were collected by our grower cooperators (sample size: 139). The same protocol was utilized by two laboratories to analyze samples (Lincoln et al., 2019; Mundorf et al., 2015). Tissue samples were dried at 65 °C for at least 72 h and then ground through a 0.25-mm mesh screen. The Dumas combustion method was used to determine foliar nitrogen concentration. For other nutrients, ground samples were digested with nitric acid and hydrogen peroxide, and were then analyzed on inductively coupled plasma optimal emission spectrometers.

Table 1
Data used in the project.

A) Dry leaf spectra

Dates	Old leaves	New leaves	Sensor specifications
2018–07-03	81	81	Sensor: ASD FieldSpec4
2019–06-26	75	75	Spectral range: 350–2500 nm
2019–09-04	50 (no leaf separation)		Interpolated spectral interval: 1 nm
2021–06-22	24	24	

B) Foliar nutrients

Brookside Laboratories			Midwest Laboratories		Foliar nutrients
Dates	Old leaves	New leaves	Dates	Samples	
2018–07-03	18	18	2018–08-15	52	N, P, K, Mg, Ca, S, Na, Fe, Mn, B, Cu, Zn, in $mg \bullet g^{-1}$
2019–06-26	10	10	2019–08-15	44	
2019–09-04	26 (no leaf separation)		2020–08-15	49	
2021–06-22	24	24	2021–08-15	46	

C) Canopy spectra

Dates	Samples	Image specifications
2018–07-02	80	Sensors: HySpex VNIR-1800, SWIR-384
2019–06-25	76	Spectral range: 400–1000 nm, 930–2500 nm
2019–08-29	32	Spectral bands: 186, 288
2020–08-20	42	Spectral resolution: 3.26 nm, 5.45 nm
2021–06-19	12	Flying height: 2100 *m*
		Spatial resolution: 0.75 m, 1.50 *m*

c) Canopy spectra

Canopy spectra were collected on five dates using two co-aligned HySpex VNIR-1800 and SWIR-384 imaging spectrometers (Norsk Elektro Optikk, Oslo, Norway) ("Canopy spectra" in Table 1). The VNIR-1800 measures 186 spectral bands between 400 and 1000 nm with a spectral resolution of 3.26 nm. The SWIR-384 measures 288 spectral bands between 930 and 2500 nm with a resolution of 5.45 nm. The HySpex instruments were flown on a Cessna-180 airplane between 11:00 a.m. and 13:30p.m. local time at an above-ground height of 2100 m, generating a pixel size of 0.75 m for VNIR-1800 images and 1.50 m for SWIR-384 images.

HySpex images were pre-processed using two open-source packages: HyPro (Liu et al., 2019) and HyTools (Queally et al., 2022; Wang et al., 2020). The processing steps included: 1) sensor boresighting; 2) radiometric calibration; 3) smile-effect correction; 4) geometric correction; 5)

atmospheric correction; 6) BRDF (Bidirectional Reflectance Distribution Function) correction; and 7) vector normalization. For more details, please refer to (Liu et al., 2021). Noisy bands and atmospheric water-absorption bands at 400–520, 920–1000, 1340–1500, 1800–2020 and 2300–2500 nm were excluded.

3. Methods

3.1. Foliar nutrient modelling at leaf and canopy scales

Four data-driven regression approaches, including partial least square regression (PLSR), support vector regression (SVR), Gaussian process regression (GPR) and random forest regression (RFR), were used to link foliar nutrients with either ASD dry leaf reflectance or canopy reflectance from the HySpex imaging spectrometer. These methods have been used to model foliar biochemistry and select informative spectral bands (Feilhauer et al., 2015; Pullanagari et al., 2021, 2016; Verrelst et al., 2016; Wang et al., 2020, 2015).

a) Datasets for modelling

At the leaf scale, 130 measurements of foliar nutrients and dry leaf spectra were used to build models ("Dry leaf spectra" and "Brookside Laboratories" in Table 1). Only the shortwave infrared reflectance (wavelength range: 1400–2500 nm) was used for modelling (Wang et al., 2020). At the canopy scale, 237 measurements of foliar nutrients and canopy spectra were used to build models ("Brookside Laboratories" and "Midwest Laboratories" and "Canopy spectra" in Table 1). The foliar nutrients of old and new leaves on 2018–07-03, 2019–06-26 and 2021–06-22 were averaged using their dry weights ("Brookside Laboratories" in Table 1):

$$C_{\text{cranberry upright}} = \frac{W_{\text{old}} C_{\text{old}} + W_{\text{new}} C_{\text{new}}}{W_{\text{old}} + W_{\text{new}}}$$

where W_{old} and W_{new} are the dry weights of old and new leaves respectively; C_{old} and C_{new} are the nutrient concentrations of old and new leaves respectively; $C_{\text{cranberry upright}}$ is the nutrient concentration of a whole cranberry upright. The original dataset was 3:1 randomly split into calibration and validation datasets.

b) Parameter optimization and model calibration.

Model parameters were set or optimized prior to model calibration (Table 2). The settings or optimization ranges of model parameters were adopted from previous studies (Feilhauer et al., 2015; Pullanagari et al., 2021, 2016; Wang et al., 2020, 2015). For PLSR, the number of latent factors (h) was optimized from 1 to 20 with a step size of one. For SVR, the kernel function was set to the radial basis function; the regularization parameter (C) was exponentially optimized from 2^{-15} to 2^{16}; the kernel coefficient (γ) was exponentially optimized from 2^{-5} to 2^{6}; the penalty coefficient (ε) was exponentially optimized from 10^{-5} to 10^{4}. For GPR, the kernel function was set to the radial basis function. For RFR, the number of decision trees (n_{tree}) was set to 500 (Belgiu et al., 2016; Lawrence et al., 2006); the number of features (m_{try}) was optimized from 1 to $p/3$ (p: the number of spectral bands) with a step size of five.

Table 2
The settings and optimization ranges of model parameters.

Models	Parameters	Setting/Optimization range
Partial least square regression (PLSR)	Number of latent factors (h)	1, 2, …, 20
Support vector regression (SVR)	Kernel function	Radial basis function
	Regularization parameter (C)	2^{-15}, 2^{-14}, …, 2^{16}
	Kernel coefficient (γ)	2^{-5}, 2^{-4}, …, 2^{6}
	Penalty coefficient (ε)	10^{-5}, 10^{-4}, …, 10^{4}
Gaussian process regression (GPR)	Kernel function	Radial basis function
Random forest regression (RFR)	Number of decision trees (n_{tree})	500
	Number of features randomly sampled as candidates at each split (m_{try})	1, 6, …, $p/3$ (p: the number of spectral bands)

The optimization of model parameters was accomplished using a repeated k-fold cross-validation strategy: 1) The calibration dataset was randomly split into 4 folds, with 3 folds randomly chosen for training and the fourth for testing; 2) The training dataset was used to build models for a given set of parameter values (e.g., C=2^{-4}, γ=2^{3} and$\varepsilon = 10^{2}$ in SVR); 3) The trained models were applied to the testing dataset to predict foliar nutrients; 4) Steps 1–3 were repeated 100 times to generate 100 estimations for each data point for a given set of parameter values; 5) The set of parameter values that produced the lowest prediction error was chosen as the optimal parameters (Chlus and Townsend, 2022; Wang et al., 2020).

With the optimal model parameters, foliar nutrient models were calibrated by applying the repeated k-fold cross-validation (4 folds, 25 repeats) strategy to the calibration dataset again. This was done to reduce the influence of data sampling on model calibration. Therefore, there were 100 prediction models for each data-driven approach.

c) Model evaluation

Calibrated models produced 100 predictions for each data point in each validation dataset. The average of 100 model predictions was used as the model estimation of each data point and the standard deviation was used as the estimation uncertainty. Model performance was evaluated using the coefficient of determination (R^2), root mean squared error (RMSE, in mg•g^{-1}) and relative RMSE (RRMSE, = RMSE/(Max-Min)× 100%, in %).

3.2. Exploration of the physical basis of hyperspectral remote sensing of foliar nutrients

We explored the physical basis of hyperspectral remote sensing of foliar nutrients by: 1) selecting and analyzing the spectral bands that are important for modelling foliar nutrients; and 2) investigating the correlation between foliar nutrients and leaf compounds that have strong absorption features. Our analysis steps are as follows:

a) Selection and analysis of important spectral bands

We adopted the procedure to select important spectral bands reported by Wang et al. (2019; see also Fig. 2). For each data-driven approach, the absolute model coefficients, characterizing the relative importance of each band to the prediction of foliar nutrients, were ranked in descending order across wavelengths (Table 3). Then, the top 30% ranked bands were selected as important bands (vertical lines in Fig. 2A). Since there were 100 model runs for each data-driven approach (see Section 3.1.b), the procedure of band ranking and selection was repeated 100 times (Fig. 2A). Finally, the frequency of each band being selected by models was calculated (frequency range: 0–100, Fig. 2B). The more frequently a spectral band was selected by models, the more important/informative this band was.

Some spectral bands are located at the absorption features of leaf compounds such as leaf chlorophyll, water and dry matters (protein, nitrogen, lignin, cellulose, sugar, starch and oil) (Curran, 1989). Previous studies have suggested that the absorption features of these leaf compounds are likely leveraged by models to predict foliar nutrients (Chlus and Townsend, 2022; Mutanga et al., 2005; Pandey et al., 2017; Pullanagari et al., 2016). Therefore, the selection frequency (or importance) at these absorption features was analyzed to explore the physical

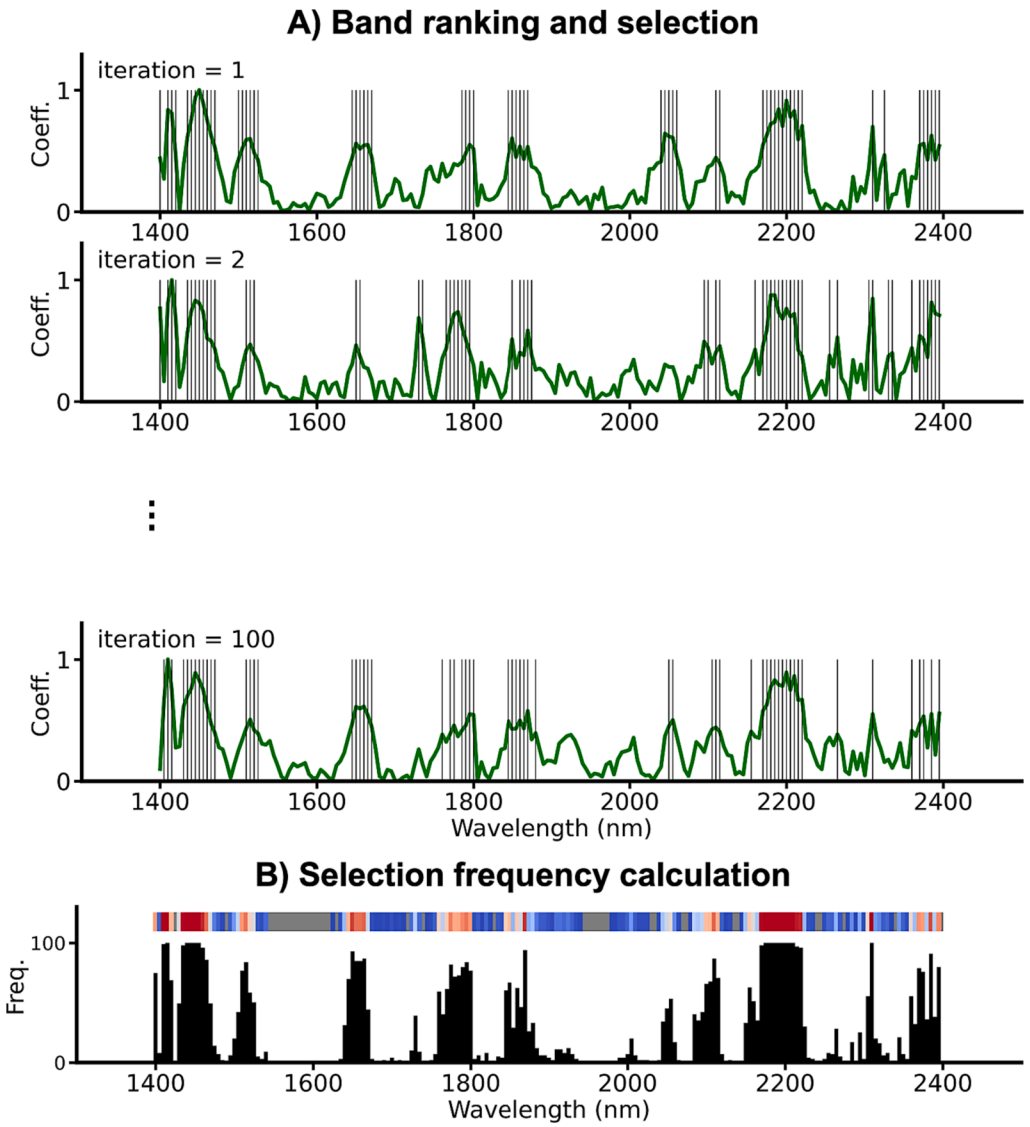

Fig. 2. An example of calculating the selection frequency for each spectra band. In panel A, the prediction model is run 100 times for a foliar nutrient using the repeated k-fold cross validation (iteration = 1, 2, …, 100); The top 30% bands (vertical lines) are selected by ranking the absolute model coefficients (green curves) in each model run. In panel B, vertical bars show the frequency of each band being selected by 100 models; The horizontal bar provides another way to visualize the selection frequency, with blue colors representing a low frequency, red colors representing a high frequency and the grey color representing no band selection. (For interpretation of the references to color in this figure legend, the reader is referred to the web version of this article.)

Table 3
The model coefficients used to rank the importance of spectral bands.

Models	Coefficients	References
Partial least square regression (PLSR)	Standardized coefficients	(Chlus and Townsend, 2022)
Support vector regression (SVR)	The inner product of spectral reflectance and the α-vector	(Feilhauer et al., 2015)
Gaussian process regression (GPR)	The inverse of the length-scale vector	(Wang et al., 2019)
Random forest regression (RFR)	Feature importance coefficients	(Feilhauer et al., 2015)

basis of foliar nutrient remote sensing in the following analysis. For the positions of these leaf compound absorption features, please refer to (Curran, 1989). In summary, there are 12 absorption features within the visible-to-near infrared (VNIR) wavelength range (400–1200 nm), 30 features within the shortwave infrared (SWIR) wavelength range (1400–2500 nm).

b) The correlation between foliar nutrients and leaf compounds

We calculated the Pearson's correlation between foliar nutrients and leaf compounds such as leaf chlorophyll, water and dry matters (LMA (leaf mass per area, in g•cm^{-2}), protein, lignin, cellulose, sugar and starch (in mg•g^{-1})). In this study, we did not measure leaf compounds due to cost reasons. Alternatively, we used dry leaf spectra to estimate leaf dry matters, and used vegetation indices as surrogates of leaf chlorophyll, water and canopy LAI (Leaf Area Index).

1) *Leaf dry matters*: In previous studies, we measured leaf dry matters (LMA, lignin, cellulose, sugar and starch) and dry leaf spectra for 184 plant species sampled from seven NEON (National Ecological Observatory Network) domains in the US (Wang et al., 2022, 2020). This dataset covered a wide range of leaf types with ~ 700 samples. Using this dataset, we built PLSR models to link leaf dry matters with dry leaf spectra. These models were then applied to our dry leaf spectra data ("Dry leaf spectra" in Table 1) to estimate leaf dry matters. Considering that nitrogen is mainly bound within proteins, a

conversion factor of 4.43 was applied to our nitrogen data to estimate proteins (Berger et al., 2020).

2) *Leaf chlorophyll, water and canopy LAI*: Two vegetation indices, TCARI/OSAVI and NDWI calculated from canopy spectra ("Canopy spectra" in Table 1), were used as surrogates of leaf chlorophyll and water, respectively. The ratio TCARI/OSAVI (TCARI: Transformed Chlorophyll Absorption in Reflectance Index; OSAVI: Optimized Soil Adjusted Vegetation Index) has been found to be sensitive to leaf chlorophyll but resistant to canopy LAI (Leaf Area Index) (Haboudane et al., 2002). The NDWI (Normalized Difference Water Index) has been found to be sensitive to leaf water (Gao, 1996). We also tested other vegetation indices that were sensitive to leaf chlorophyll and water (Table S-1). In general, these indices were found to highly correlate with TCARI/OSAVI and OSAVI (Figure S-1). In addition, we used NDVI as a surrogate of canopy LAI (leaf area index, in m^{-2}• m^{-2}).

At leaf scales, the correlation between foliar nutrients and leaf dry matters (LMA, lignin, cellulose, sugar and starch) was calculated. At canopy scales, the correlation of foliar nutrients with dry matters (LMA, lignin, cellulose, sugar and starch), TCARI/OSAVI (as a surrogate of leaf chlorophyll), NDWI (leaf water), and NDVI (canopy LAI) was calculated. The dry matters derived from dry leaf spectra for new and old growth leaves were upscaled to canopy scales using dry leaf weights before the canopy-scale correlation analysis.

4. Results

4.1. Comparison of model performance among the four regression methods

At leaf scales, PLSR and SVR performed better than GPR and RFR for nutrient predictions (Table 4A). Among the 12 foliar nutrients, PLSR and SVR showed the best performance for nine nutrients, whereas GPR and RFR performed best only for three nutrients (highlighted in green). More specifically, PLSR produced the best results for leaf Mg (validation R^2 = 0.54, RRMSE = 9%), Ca (R^2 = 0.85, RRMSE = 10%), Fe (R^2 = 0.69, RRMSE = 48%) and Zn (R^2 = 0.30, RRMSE = 26%); SVR produced the best results for leaf P (R^2 = 0.93, RRMSE = 11%), S (R^2 = 0.74, RRMSE = 10%), Na (R^2 = 0.58, RRMSE = 32%), B (R^2 = 0.84, RRMSE = 13%) and Cu (R^2 = 0.66, RRMSE = 20%); GPR produced the best results for leaf N (R^2 = 0.88, RRMSE = 12%) and K (R^2 = 0.89, RRMSE = 11%); RFR produced the best results only for leaf Mn (R^2 = 0.54, RRMSE = 51%). In general, the poorest results were produced by RFR for most macronutrients and by GPR for most micronutrients (highlighted in yellow in Table 4A).

At canopy scales, PLSR performed best in predicting foliar nutrients, followed by GPR, SVR and RFR (Table 4B). PLSR produced the best results for seven foliar nutrients, including leaf K (R^2 = 0.25, RRMSE = 7%), Ca (R^2 = 0.75, RRMSE = 10%), Na (R^2 = 0.80, RRMSE = 14%), Fe (R^2 = 0.60, RRMSE = 37%), Mn (R^2 = 0.15, RRMSE = 28%), B (R^2 = 0.54, RRMSE = 20%) and Zn (R^2 = 0.48, RRMSE = 16%). GPR produced

Table 4
The performance of the four models in predicting cranberry foliar nutrients at leaf and canopy scales. For each foliar nutrient, the best model is highlighted in green, and the poorest model is in yellow. ΔR^2 and ΔRRMSE are the differences in R^2 and RRMSE between the best (green) and poorest (yellow) models, respectively. *n*: validation dataset size; PLSR: partial least squared regression; SVR: support vector regression; GPR: Gaussian process regression; RFR: random forest regression. For the scatterplot results of each foliar nutrient, please refer to Figures S-2 and S-3.

A) Model validation at leaf scales (n = 32)

Macronutrients	*PLSR*		*SVR*		*GPR*		*RFR*		*Best-Poorest*	
	R^2	*RRMSE*	R^2	*RRMSE*	R^2	*RRMSE*	R^2	*RRMSE*	ΔR^2	Δ*RRMSE*
N	0.86	12%	0.83	14%	0.88	12%	0.68	19%	0.20	−7%
P	0.88	11%	0.93	11%	0.89	12%	0.75	16%	0.18	−1%
K	0.85	12%	0.88	11%	0.89	11%	0.83	13%	0.06	−2%
Mg	0.54	9%	0.51	10%	0.26	12%	0.28	12%	0.28	−3%
Ca	0.85	10%	0.82	11%	0.79	12%	0.74	14%	0.11	−4%
S	0.67	11%	0.74	10%	0.74	12%	0.59	14%	0.15	−4%
Na	0.53	33%	0.58	32%	0.52	34%	0.41	35%	0.17	−3%
Micro nutrients	***PLSR***		***SVR***		***GPR***		***RFR***		***Best-Poorest***	
	R^2	*RRMSE*	R^2	*RRMSE*	R^2	*RRMSE*	R^2	*RRMSE*	ΔR^2	Δ*RRMSE*
Fe	0.69	48%	0.68	50%	0.64	55%	0.68	52%	0.05	−7%
Mn	0.41	64%	0.50	56%	0.53	51%	0.54	51%	0.13	−13%
B	0.78	16%	0.83	13%	0.38	26%	0.46	24%	0.46	−13%
Cu	0.62	21%	0.66	20%	0.57	23%	0.56	23%	0.10	−3%
Zn	0.30	26%	0.23	27%	0.01	31%	0.03	31%	0.30	−5%

B) Model validation at canopy scales (n = 61)

Macro nutrients	*PLSR*		*SVR*		*GPR*		*RFR*		*Best-Poorest*	
	R^2	*RRMSE*	R^2	*RRMSE*	R^2	*RRMSE*	R^2	*RRMSE*	ΔR^2	Δ*RRMSE*
N	0.75	13%	0.81	11%	0.79	11%	0.79	11%	0.06	−2%
P	0.45	8%	0.47	7%	0.50	7%	0.44	7%	0.06	0%
K	0.25	7%	0.20	7%	0.20	7%	0.21	7%	0.05	0%
Mg	0.73	10%	0.68	10%	0.73	9%	0.71	9%	0.05	−1%
Ca	0.75	10%	0.70	11%	0.74	10%	0.71	10%	0.05	−1%
S	0.52	14%	0.62	12%	0.63	11%	0.61	12%	0.11	−3%
Na	0.80	14%	0.77	15%	0.75	15%	0.71	17%	0.09	−3%
Micro nutrients	***PLSR***		***SVR***		***GPR***		***RFR***		***Best-Poorest***	
	R^2	*RRMSE*	R^2	*RRMSE*	R^2	*RRMSE*	R^2	*RRMSE*	ΔR^2	Δ*RRMSE*
Fe	0.60	37%	0.46	44%	0.43	44%	0.44	43%	0.17	−7%
Mn	0.15	28%	0.01	28%	0.08	27%	0.12	26%	0.14	0%
B	0.54	20%	0.45	22%	0.51	20%	0.46	21%	0.09	−2%
Cu	0.46	16%	0.39	17%	0.50	15%	0.39	17%	0.11	−2%
Zn	0.48	16%	0.38	18%	0.45	17%	0.42	17%	0.10	−2%

the best results for five foliar nutrients, including leaf P (R^2 = 0.50, RRMSE = 7%) and Mg (R^2 = 0.73, RRMSE = 9%), S (R^2 = 0.63, RRMSE = 11%) and Cu (R^2 = 0.50, RRMSE = 15%). SVR produced the best results only for leaf (R^2 = 0.81, RRMSE = 11%). RFR did not produce the best results for any foliar nutrient. It should be noted that the improvement in prediction accuracy from the poorest to the best models was quite small at canopy scales (ΔR^2 and ΔRRMSE in Table 4B). For most foliar nutrients, ΔR^2 and ΔRRMSE were<0.1 and 5%, respectively. Only leaf Fe had a ΔR^2>0.1 (ΔR^2 = 0.17) and ΔRRMSE>5% (ΔRRMSE = 7%).

Macronutrients generally had a higher prediction accuracy than micronutrients. At leaf scales, most macronutrients had a validation RRMSE<15%, whereas the RRMSE of most micronutrients ranged from 20 to 65% (Table 4A). At canopy scales, all macronutrients had a validation RRMSE<15%, whereas the RRMSE of all micronutrients ranged from 15 to 37% (Table 4B). For the scatterplot results, please refer to Figures S-2 and S-3.

4.2. Selection frequency at the strong absorption features of leaf compounds

With the exception nitrogen, most nutrients do not have strong absorption features within 400–2500 nm. For these elements, some of the frequently selected bands (selection frequency ≥ 50 times) were found to be around the documented absorption features of leaf compounds such as chlorophyll, water, and dry matters (nitrogen, protein, lignin, starch, cellulose and sugar) (Table 5). For example, the leaf-scale SVR models for phosphorus frequently selected seven absorption features, with 1420 nm being around the absorption feature of lignin, 1900 nm around starch, 1980, 2130 and 2240 nm around protein, 2310 nm around oil, and 2320 nm around sugar (Table 5A). The canopy-scale PLSR models for calcium frequently selected three absorption features, with 910 nm being around the absorption feature of nitrogen, 1690 nm around nitrogen, protein, lignin and starch, and 2320 nm around starch (Table 5B).

4.3. The correlation between foliar nutrients and leaf compounds

At leaf scales, LMA most correlated with foliar nutrients (Fig. 3A). With the exception of Mg, S, B and Zn, the absolute Pearson's correlation coefficient $|r|$ between LMA and foliar nutrients ranged from 0.63 to 0.87. Negative correlations were observed between LMA and N, P, K, Mg, S, Cu and Zn ($|r| > 0.6$ in general), whereas positive correlations were observed for Ca, Na, Fe, Mn and B ($|r| > 0.65$). When dry matters were decomposed into various leaf compounds, protein most correlated with foliar nutrients ($|r| > 0.5$), followed by sugar, cellulose, lignin and starch ($|r| < 0.4$).

At canopy scales, TCARI/OSAVI (as a surrogate of leaf chlorophyll) and NDVI (as a surrogate of canopy LAI) most correlated with foliar nutrients (the absolute Pearson's correlation value $|r| > 0.6$ generally), followed by NDWI (as a surrogate of leaf water, $|r|$ = 0.4–0.55) and LMA ($|r| < 0.5$) (Fig. 3B). Among leaf dry compounds, protein most correlated with foliar nutrients ($|r|$ = 0.5–0.76), followed by cellulose ($|r|$ = 0.4–0.5), and lignin, sugar and starch ($|r| < 0.4$). It was also noticed that the correlation of foliar nutrients with LMA, lignin, sugar and starch was weakened from leaf to canopy scales. On average, the absolute correlation coefficient $|r|$ was decreased by ~ 0.2 during the upscaling.

4.4. Cranberry nutrient concentration mapping

Spatial variations in foliar nutrients were observed across and within cranberry beds (Fig. 4). For example, some cranberry beds at locations A and B had a nitrogen concentration lower than 11 mg•g^{-1}, whereas the cranberry beds at location C had a nitrogen concentration higher than 15 mg•g^{-1}. At location D, the nitrogen concentration at the edge of cranberry beds was apparently lower than that in the middle of beds.

Table 5
The spectral bands with a selection frequency ≥ 50 times by the best leaf- or canopy-scale models and with a location around the absorption features of leaf compounds. Letters a-I indicate the leaf compounds that have absorption features at each wavelength. PLSR: partial least squared regression; SVR: support vector regression; GPR: Gaussian process regression; RFR: random forest regression.

A) Leaf-scale models

Foliar nutrients	Best model	Wavelengths (nm)	Leaf compounds
N	GPR	1420[c], 1450[c,d,f], 1490[e,f]	a: nitrogen
P	SVR	1420[c], 1900[d], 1980[b], 2130[b], 2240[b], 2310 [g], 2320[f]	b: protein c: lignin
K	GPR	1420[c]	d: starch
Mg	SVR	1690[a,b,c,d], 1900[d], 1940[a,b,c,d,e], 1980[b], 2000[d], 2130[b], 2240[b], 2270[d,e,f], 2280[e,f], 2350[a,b,e]	e: cellulose f: sugar g: oil
Ca	PLSR	1900[d], 1940[a,b,c,d,e], 2000[d], 2240[b], 2250[d], 2270[d,e,f], 2280[d,e], 2310 [g], 2350[a,b,e]	
S	SVR	1420[c], 1450[c,d,f], 1580[d,f], 2130[b], 2240[b]	
Na	SVR	1420[c], 1820[e], 1960[d,f], 1980[b], 2060[a,b]	
Fe	PLSR	1420[c], 1820[e], 2130[b], 2180[a,b], 2240[b], 2250[d], 2310 [g], 2320[d], 2350[a,b,e]	
Mn	RFR	1580[d,f], 1690[a,b,c,d], 1780[d,e,f], 1820[e]	
B	SVR	1960[d,f], 2000[d], 2240[b], 2270[d,e,f], 2320[d], 2350[a,b,e]	
Cu	SVR	1420[c], 1580[d,f], 1980[b], 2060[a,b], 2080[d,f], 2100[d,e], 2130[b], 2240[b], 2250[d]	
Zn	PLSR	1420[c], 1900[d], 1960[d,f], 1980[b], 2000[d], 2130[b]	

B) Canopy-scale models

Foliar nutrients	Best model	Wavelengths (nm)	Leaf compounds
N	SVR	910[b], 1020[b], 1120[c]	a: nitrogen
P	GPR	None	b: protein
K	PLSR	910[b], 1120[c], 2100[d,e]	c: lignin
Mg	GPR	2320[d]	d: starch
Ca	PLSR	910[b], 1690[a,b,c,d], 2320[d]	e: cellulose
S	GPR	2080[d,f], 2100[d,e], 2130[b], 2180[a,b]	f: sugar
Na	PLSR	1020[b], 1040[i], 1690[a,b,c,d], 1780[d,e,f], 2310 [g], 2320[d]	g: oil h: chlorophyll
Fe	PLSR	1020[b], 2060[a], 2080[d,f], 2310 [g]	i: water
Mn	PLSR	1120[b], 1510[a,b], 1530[d], 1690[a,b,c,d], 2080[d,f], 2280[d,e], 2310 [g]	
B	PLSR	910[b], 1780[d,e,f], 2270[d,e,f], 2320[d]	
Cu	GPR	2080[d,f], 2130[b]	
Zn	PLSR	660 [h], 1020[b], 1040 [g], 1120[c]	

Negative predictions at low concentrations were produced by the models for leaf Fe and B (blank cranberry beds at location A for iron and boron, Figures S-4 and S-5). Similar spatial distribution patterns were observed among some nutrients (e.g., N, Mg, Ca, S and B) due to their strong intercorrelations (Pearson's correlation range: 0.70–0.80).

It should also be noted that the foliar nutrient maps presented here were produced using the range of model predictions. Therefore, a low (or high) concentration value on maps does not necessarily indicate that cranberry plants are under nutrient deficiency (or excess). To diagnose the nutrient status of cranberries, normal nutrient ranges need to be applied to these maps (Davenport et al., 1995). For example, all the cranberry beds mapped here actually had a nitrogen concentration above normal (=7.5 mg•g^{-1}), and were classified as "High-to-Excessive" by Midwest Laboratories, suggesting that the amount of nitrogen fertilizer should be reduced next year.

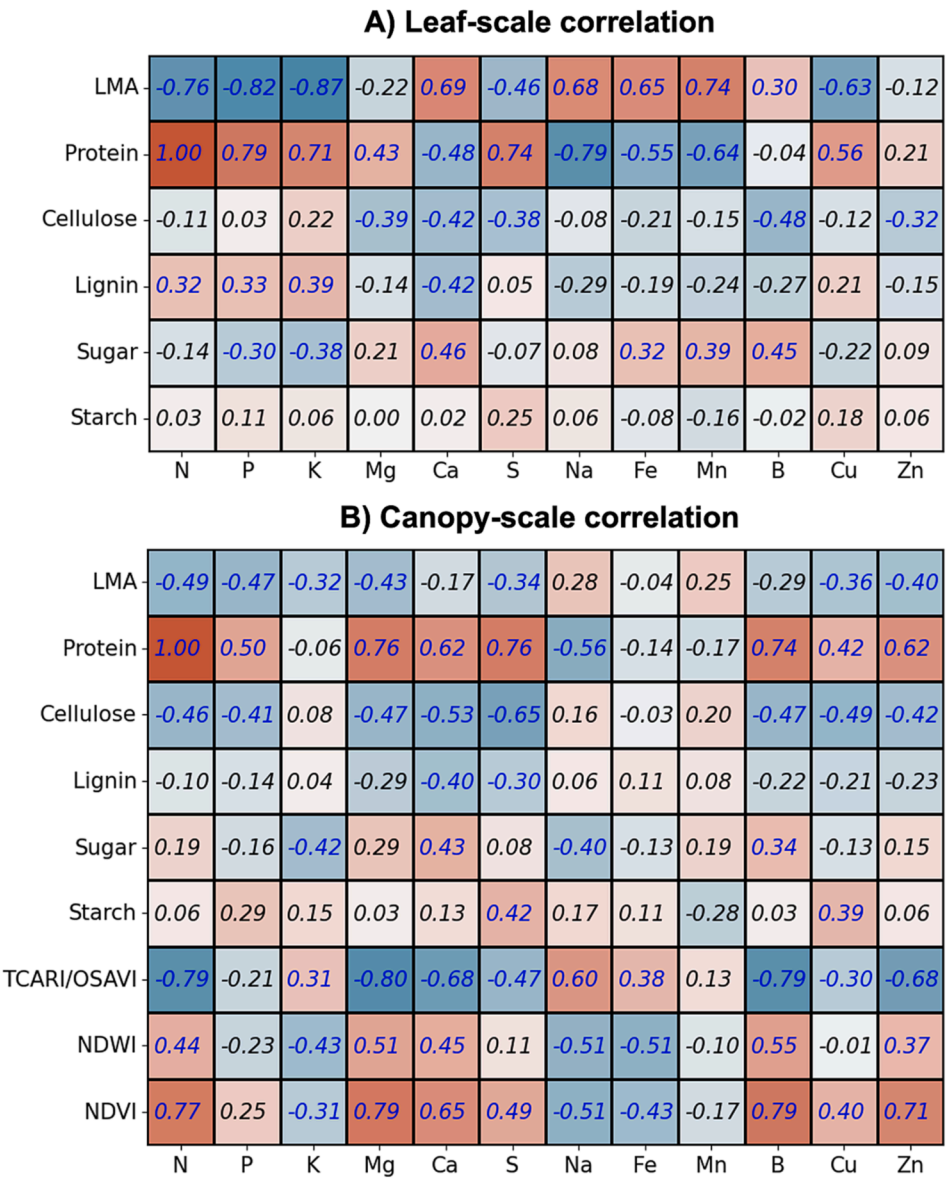

Fig. 3. The Pearson's correlation coefficient between foliar nutrients and leaf compounds. Panel A shows the correlation between foliar nutrients and leaf dry matters (LMA, protein, lignin, cellulose, sugar and starch) at leaf scales. Panel B shows the correlation of foliar nutrients with dry matters (LMA, lignin, cellulose, sugar and starch, derived from dry leaf spectra), TCARI/OSAVI (as a surrogate of leaf chlorophyll), NDWI (leaf water), and NDVI (canopy LAI) at canopy scales. Correlations with an absolute value>0.3 were highlighted in blue. The correlation between leaf protein and nitrogen is always one because Protein = 4.43 × leaf N. (For interpretation of the references to color in this figure legend, the reader is referred to the web version of this article.)

5. Discussion

5.1. Selecting appropriate data-driven approaches for modelling foliar nutrients

The observation that linear approaches (PLSR and SVR) outperformed nonlinear approaches (GPR and RFR) at leaf scales (Table 4A) has also been noted by Feilhauer et al. (2015) who attempted to estimate leaf chlorophyll, water and dry matter contents from leaf reflectance. The less encouraging results of GPR and RFR could be attributed to overfitting, which is most commonly diagnosed when models performed much better with the calibration dataset than the validation dataset. In general, SVR performed slightly better than PLSR. Among the 12 foliar nutrients, SVR had a higher R^2 for eight nutrients. This was likely because a nonlinear relationship between foliar nutrients and spectra is embedded in the RBF (radial basis function) transformation of raw spectra in SVR (Feilhauer et al., 2015; Zhai et al., 2013). In our case, it appears that SVR and PLSR are best suited to model foliar nutrients at leaf scales.

Nonlinear approaches did not significantly improve the prediction accuracy at canopy scales, which was a surprise. Being affected by many confounding factors (e.g., canopy structures and soil background), the relationship between leaf biochemicals and canopy reflectance tends to be complicated and nonlinear (Verrelst et al., 2015, 2012). Therefore, nonlinear approaches generally outperformed linear approaches at canopy scales in previous studies (Axelsson et al., 2013; Pullanagari et al., 2016; Ramoelo et al., 2013). However, in our case the difference in prediction accuracy between linear and nonlinear approaches was quite small ($\Delta R^2 < 0.1$ and $\Delta RRMSE < 5\%$, Table 4B). Considering that PLSR has a low complexity but a comparative performance, this approach appears to be the optimal choice for modelling cranberry foliar nutrients at canopy scales.

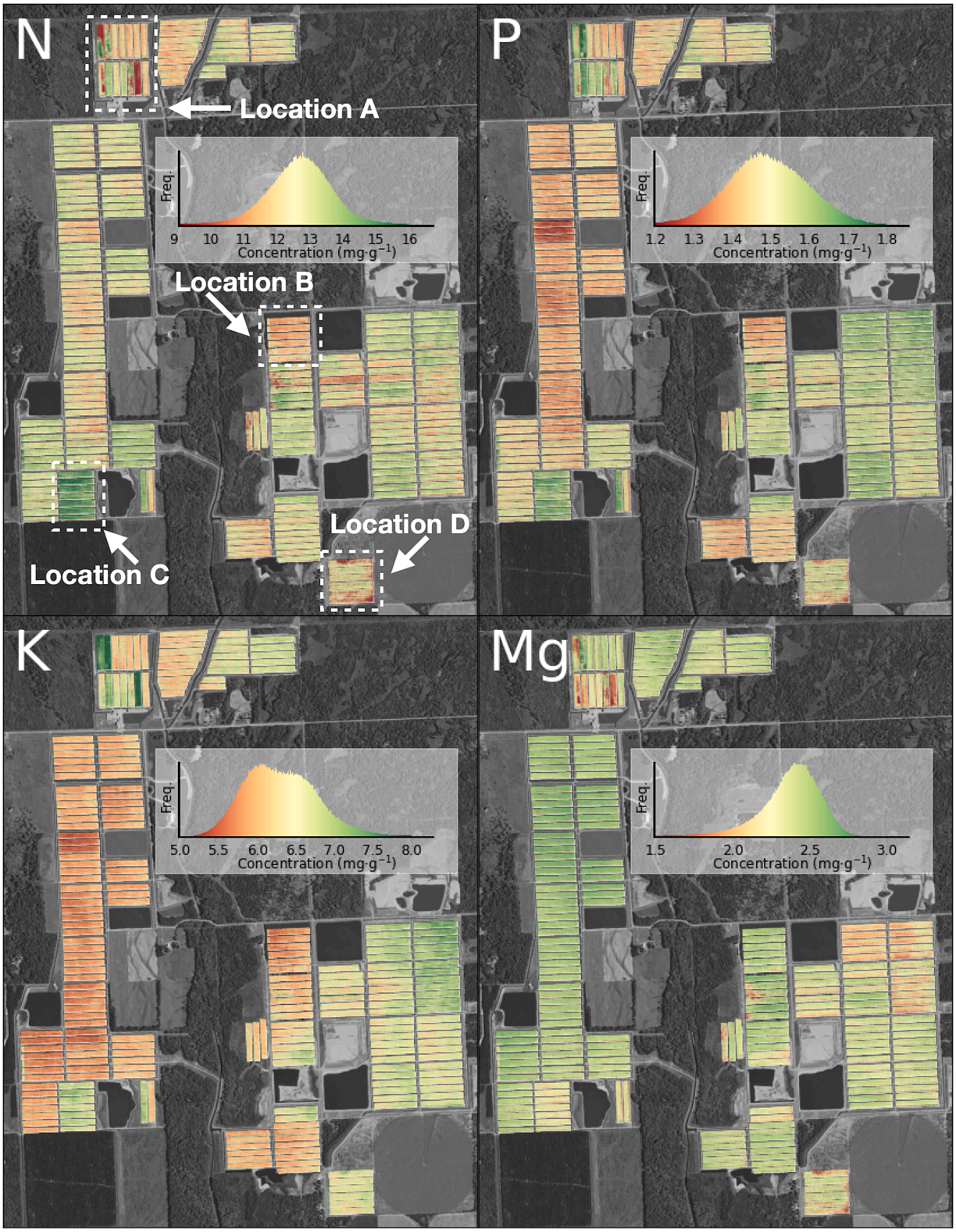

Fig. 4. Cranberry nutrient concentration maps of 2020–08-20 derived from canopy reflectance acquired by Hyspex imaging spectroscopy. Only nutrients nitrogen, phosphorus, potassium and magnesium are shown here. For the mapping results of other nutrients, please refer to Figures S-4 and S-5.

5.2. The physical basis of hyperspectral remote sensing of foliar nutrients

The correlations between foliar nutrients and leaf compounds were in general agreement with previous studies (Reich 2012; Homolová et al., 2013; Wright et al., 2004; Asner et al., 2016; Dana Chadwick & Asner, 2016; Pullanagari et al., 2016). LMA was negatively correlated to nitrogen and phosphorus mainly due to the strategy of resource acquisition and storage in plants (Wright et al., 2004; Asner et al., 2016; Dana Chadwick & Asner, 2016). Magnesium and nitrogen are important elements in chlorophyll, and therefore were strongly correlated with the

chlorophyll indices TCARI/OSAVI and NDVI. Furthermore, the inter-correlation of nitrogen with other nutrients (i.e., the correlation of protein with other nutrients in Fig. 3) was also noticed in previous studies (Axelsson et al., 2013; Pullanagari et al., 2016; Abdel-Rahman et al., 2017).

The feasibility of leaf and imaging spectroscopy in estimating foliar nutrients can be explained by their correlations with leaf compounds that have strong absorption features. At leaf scales, the strong correlation of foliar nutrients with LMA (Fig. 3A) was the main reason why the absorption features of dry leaf compounds were frequently selected by models (Table 5A). For example, since phosphorus was strongly correlated with LMA (r = -0.82, Fig. 3A), its prediction models frequently leveraged the absorption features of five dry leaf compounds, including protein (1980, 2130 and 2240 nm), lignin (1420 nm), sugar (2320 nm), starch (1900 nm) and oil (2310 nm) (Table 5A). Furthermore, we found a strong positive correlation relationship ($r = 0.62$, Fig. 5A) between the performance of foliar nutrient models (R^2 in Fig. 3A) and the absolute correlation ($|r|$ in Fig. 5A) of foliar nutrients with LMA, indicating that the more a specific foliar nutrient was correlated with LMA, the better the performance of prediction models would be.

At canopy scales, the strong correlation of foliar nutrients with leaf chlorophyll and canopy LAI (TCARI/OSAVI and NDVI in Fig. 3B) explained why foliar nutrients could be estimated from canopy spectra. We found that the performance of canopy-scale nutrient models (R^2 in Fig. 5B) was positively correlated with the correlation ($|r|$ in Fig. 5B) between foliar nutrients and leaf chlorophyll ($r = 0.71$, TCARI/OSAVI in Fig. 5B) and canopy LAI ($r = 0.67$, NDVI in Fig. 5B). This finding indicated that the more a specific foliar nutrient was correlated with leaf chlorophyll or canopy LAI, the better the performance of prediction models would be. The insignificant correlation between R^2 and $|r|$ for leaf water ($r = 0.46$, $P = 0.13$, NDWI in Fig. 5B) and LMA ($r = 0.08$, $P = 0.79$, LMA in Fig. 5B) suggested that at canopy scales the absorption features of leaf water and dry matters were not as important as that of leaf chlorophyll and canopy LAI in modelling foliar nutrients.

5.3. Challenges in hyperspectral mapping of foliar nutrients

Some challenges remain in utilizing imaging spectroscopy to quantify foliar nutrients at canopy scales. Canopy reflectance is affected by many other factors such as the sun-view geometry, atmosphere conditions and substrate background reflectance. In cranberries, this includes varying irrigation practices, both seasonally and among varieties. The sun-view geometry can induce the BRDF (Bidirectional Reflectance Distribution Function) effect, that is, the observed canopy reflectance changes with the positions of the sun and sensors (Queally et al., 2022; Song et al., 2016). Atmospheric scattering and absorption affect the radiance received by sensors, and may result in systematic differences in canopy reflectance across dates (Liu et al., 2021). Cranberries require large amounts of water under hot, dry or windy weather conditions (Caron et al., 2017). An irrigation practice can substantially decrease the short infrared wavelength reflectance (1400–2500 nm) due to the strong absorption of surface water. Addressing these confounding factors imperfectly can lead to a discrepancy in canopy reflectance, thereby influencing the canopy-scale modelling, especially by incorporating the effects of these factors into the model. For example, we examined the transferability of canopy-scale models across dates using subsets of data from four dates for model calibration and the remaining date for validation. The models performed poorly in predicting foliar nutrients on the missing date (results not shown), which indicates that these data-driven approaches must utilize data covering all possible conditions for mapping to be robust for application to new dates. In this case, the effects of imperfect image preprocessing likely propagated to the foliar nutrient modelling.

It is suggested to improve the transferability of foliar nutrient models via transfer learning and active learning in the future. Transfer learning aims to reuse the knowledge gained from tasks for which a large amount

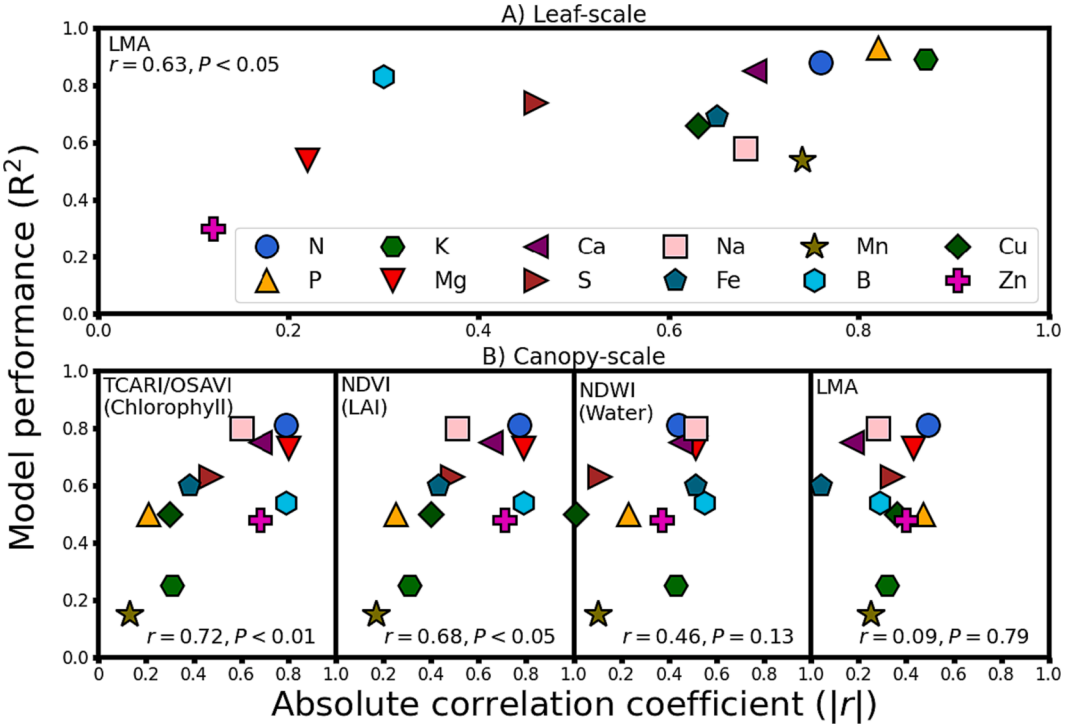

Fig. 5. The relation between the best model performance for foliar nutrients (i.e., R^2s highlighted in green in Table 4) and the absolute Pearson's correlation of foliar nutrients with leaf compounds (|r| in Fig. 3). In panel A, the absolute Pearson's correlation |r| is calculated between foliar nutrients and LMA at leaf scales (i.e., |r| for LMA in Fig. 3A). In panel B, |r| values are calculated between foliar nutrients and TCARI/OSAVI (a surrogate of chlorophyll), NDVI (LAI), NDWI (water) and LMA at canopy scales, respectively (i.e., |r| for TCARI/OSAVI, NDVI, NDWI and LMA in Fig. 3B). The r value in each panel shows the Pearson's correlation between R^2 and |r|. (For interpretation of the references to color in this figure legend, the reader is referred to the web version of this article.)

of labelled data is available in tasks where only little labelled data is available (Kganyago et al., 2022; Pan and Yang, 2010; Wan et al., 2022; Zhang et al., 2021). Active learning aims to intelligently select a small set of representative samples for model calibration (Berger et al., 2021; Settles, 2010; Upreti et al., 2019; Verrelst et al., 2021). In order to improve the transferability of foliar nutrient models across dates (or sites), it is suggested to: 1) apply transfer learning techniques to transfer the foliar nutrient models learned from previous years (or sites) to the current year (or site) so that the effects of confounding factors on the canopy-scale modelling can be reduced; 2) apply active learning techniques to select a small set of representative samples from the current year (or site) for tissue analysis, and then add these new samples into the existing calibration dataset (from previous years or sites) to recalibrate/update foliar nutrient models so that the transferability of foliar nutrient models can be improved.

6. Conclusion

We evaluated the potential of leaf and imaging spectroscopy to quantify a full range of cranberry foliar nutrients. Our results show that both leaf and imaging spectroscopies can predict cranberry foliar nutrients with a reasonable accuracy. The feasibility of leaf and imaging spectroscopy in estimating foliar nutrients was mainly due to their correlations with leaf compounds that have strong absorption features. Future efforts can be made to improve the transferability via transfer learning and active learning techniques.

Declaration of Competing Interest

The authors declare that they have no known competing financial interests or personal relationships that could have appeared to influence the work reported in this paper.

Acknowledgements

Support for this research was provided by funding to PAT from the Wisconsin State Cranberry Growers Association, the Cranberry Institute and Ocean Spray. NL received funding from GuangDong Basic and Applied Basic Research Foundation (2022A1515110575, 2023A1515011406), the Fundamental Research Funds for the Central Universities, Sun Yat-Sen University (22qntd2001), and additional funding was provided by an NSF Early NEON science grant (1638720) and NSF ASCEND Biology Integration Institute grant (DBI-2021898). Thank you to Benjamin Spaier, Joel Cryer and Cecilia Vanden Heuvel for assistance with field data collection and processing, to Williams Beckett Hills and Brendan Heberlein for assistance with remote sensing data collection and processing.

Appendix A. Supplementary material

Supplementary data to this article can be found online at https://doi.org/10.1016/j.isprsjprs.2023.10.003.

References

Abdel-Rahman, E.M., Mutanga, O., Odindi, J., Adam, E., Odindo, A., Ismail, R., 2017. Estimating Swiss chard foliar macro- and micronutrient concentrations under different irrigation water sources using ground-based hyperspectral data and four partial least squares (PLS)-based (PLS1, PLS2, SPLS1 and SPLS2) regression algorithms. Comput. Electron. Agric. 132, 21–33. https://doi.org/10.1016/j.compag.2016.11.008.

Abukmeil, R., Al-Mallahi, A.A., Campelo, F., 2022. New approach to estimate macro and micronutrients in potato plants based on foliar spectral reflectance. Comput. Electron. Agric. 198, 107074 https://doi.org/10.1016/j.compag.2022.107074.

Asner, G.P., Martin, R.E., Anderson, C.B., Knapp, D.E., 2015. Quantifying forest canopy traits: Imaging spectroscopy versus field survey. Remote Sens. Environ. 158, 15–27. https://doi.org/10.1016/j.rse.2014.11.011.

Asner, G.P., Martin, R.E., 2016. Spectranomics: Emerging science and conservation opportunities at the interface of biodiversity and remote sensing. Glob Ecol Conserv 8, 212–219. https://doi.org/10.1016/j.gecco.2016.09.010.

Axelsson, C., Skidmore, A.K., Schlerf, M., Fauzi, A., Verhoef, W., 2013. Hyperspectral analysis of mangrove foliar chemistry using PLSR and support vector regression. Int. J. Remote Sens. 34, 1724–1743. https://doi.org/10.1080/01431161.2012.725958.

Belgiu, M., Drăguţ, L., 2016. Random forest in remote sensing: A review of applications and future directions. ISPRS J. Photogramm. Remote Sens. 114, 24–31. https://doi.org/10.1016/j.isprsjprs.2016.01.011.

Berger, K., Verrelst, J., Féret, J.-B., Wang, Z., Wocher, M., Strathmann, M., Danner, M., Mauser, W., Hank, T., 2020. Crop nitrogen monitoring: Recent progress and principal developments in the context of imaging spectroscopy missions. Remote Sens. Environ. 242, 111758 https://doi.org/10.1016/j.rse.2020.111758.

Berger, K., Rivera Caicedo, J.P., Martino, L., Wocher, M., Hank, T., Verrelst, J., 2021. A survey of active learning for quantifying vegetation traits from terrestrial Earth observation data. Remote Sens. (Basel) 13, 287. https://doi.org/10.3390/rs13020287.

Bian, M., Skidmore, A.K., Schlerf, M., Wang, T., Liu, Y., Zeng, R., Fei, T., 2013. Predicting foliar biochemistry of tea (Camellia sinensis) using reflectance spectra measured at powder, leaf and canopy levels. ISPRS J. Photogramm. Remote Sens. 78, 148–156. https://doi.org/10.1016/j.isprsjprs.2013.02.002.

Caron, J., Pelletier, V., Kennedy, C.D., Gallichand, J., Gumiere, S., Bonin, S., Bland, W., Pepin, S., 2017. Irrigation and drainage management strategies to enhance cranberry production and optimize water use in North America. Can J. Soil Sci. CJSS-2016-0086. https://doi.org/10.1139/CJSS-2016-0086.

Chen, L., Zhang, Y., Nunes, M.H., Stoddart, J., Khoury, S., Chan, A.H.Y., Coomes, D.A., 2022. Predicting leaf traits of temperate broadleaf deciduous trees from hyperspectral reflectance: can a general model be applied across a growing season? Remote Sens. Environ. 269, 112767 https://doi.org/10.1016/j.rse.2021.112767.

Cheng, T., Rivard, B., Sánchez-Azofeifa, A.G., Féret, J.B., Jacquemoud, S., Ustin, S.L., 2014. Deriving leaf mass per area (LMA) from foliar reflectance across a variety of plant species using continuous wavelet analysis. ISPRS J. Photogramm. Remote Sens. 87, 28–38. https://doi.org/10.1016/j.isprsjprs.2013.10.009.

Chlus, A., Townsend, P.A., 2022. Characterizing seasonal variation in foliar biochemistry with airborne imaging spectroscopy. Remote Sens. Environ. 275, 113023 https://doi.org/10.1016/j.rse.2022.113023.

Curran, P.J., 1989. Remote sensing of foliar chemistry. Remote Sens. Environ. 30, 271–278. https://doi.org/10.1016/0034-4257(89)90069-2.

Dana Chadwick, K., Asner, G.P., 2016. Organismic-scale remote sensing of canopy foliar traits in lowland tropical forests. Remote Sens 8, 87. https://doi.org/10.3390/rs8020087.

Davenport, J.R., 1996. The effect of nitrogen fertilizer rates and timing on cranberry yield and fruit quality. J. Am. Soc. Hort. Sci. 121, 1089–1094. https://doi.org/10.21273/JASHS.121.6.1089.

Davenport, J., Demoranville, C., Hart, J., Patten, K., Peterson, L., Planer, T., Poole, A., Roper, T., Smith, J., 1995. Cranberry tissue testing for producing beds in North America. Oregon State University Extension.

De Moranville, C., 2014. Reducing phosphorus use in cranberry production: Horticultural and environmental implications. Acta Hortic. 447–453. https://doi.org/10.17660/ActaHortic.2014.1017.55.

De Moranville, C.J., Ghantous, K., 2018. 2018–2020 Chart Book: Nutrition Management. Amherst, Massachusetts, USA.

DeMoranville, C., 1992. Canberry nutrients, phenology, and N-P-K fertilization. University of Massachusetts Amherst.

Fajardo, D., Morales, J., Zhu, H., Steffan, S., Harbut, R., Bassil, N., Hummer, K., Polashock, J., Vorsa, N., Zalapa, J., 2013. Discrimination of American cranberry cultivars and assessment of clonal heterogeneity using microsatellite markers. Plant Mol. Biol. Report. 31, 264–271. https://doi.org/10.1007/s11105-012-0497-4.

Feilhauer, H., Asner, G.P., Martin, R.E., 2015. Multi-method ensemble selection of spectral bands related to leaf biochemistry. Remote Sens. Environ. 164, 57–65. https://doi.org/10.1016/j.rse.2015.03.033.

Gao, B., 1996. NDWI—A normalized difference water index for remote sensing of vegetation liquid water from space. Remote Sens. Environ. 58, 257–266. https://doi.org/10.1016/S0034-4257(96)00067-3.

Gara, T.W., Rahimzadeh-Bajgiran, P., Weiskittel, A., 2022. Determination of foliar traits in an ecologically distinct conifer species in Maine using Sentinel-2 imagery and site variables: Assessing the effect of leaf trait expression and upscaling approach on prediction accuracy. ISPRS J. Photogramm. Remote Sens. 193, 150–163. https://doi.org/10.1016/j.isprsjprs.2022.09.012.

García-Haro, F.J., Campos-Taberner, M., Moreno, Á., Tagesson, H.T., Camacho, F., Martínez, B., Sánchez, S., Piles, M., Camps-Valls, G., Yebra, M., Gilabert, M.A., 2020. A global canopy water content product from AVHRR/Metop. ISPRS J. Photogramm. Remote Sens. 162, 77–93. https://doi.org/10.1016/j.isprsjprs.2020.02.007.

Gökkaya, K., Thomas, V., Noland, T., McCaughey, H., Morrison, I., Treitz, P., 2015. Prediction of Macronutrients at the Canopy Level Using Spaceborne Imaging Spectroscopy and LiDAR Data in a Mixedwood Boreal Forest. Remote Sens. (Basel) 7, 9045–9069. https://doi.org/10.3390/rs70709045.

Haboudane, D., Miller, J.R., Tremblay, N., Zarco-Tejada, P.J., Dextraze, L., 2002. Integrated narrow-band vegetation indices for prediction of crop chlorophyll content for application to precision agriculture. Remote Sens. Environ. 81, 416–426. https://doi.org/10.1016/S0034-4257(02)00018-4.

Hagidimitriou, M., Roper, T.R., 1995. Seasonal changes in CO2 assimilation of cranberry leaves. Sci. Hortic. 64, 283–292. https://doi.org/10.1016/0304-4238(95)00835-7.

Harbut, R., 2011. Diagnosing Nutritional Status of Fruit Crops. Madison, Wisconsin, USA.

Homolová, L., Malenovský, Z., Clevers, J.G.P.W., García-Santos, G., Schaepman, M.E., 2013. Review of optical-based remote sensing for plant trait mapping. Ecol. Complex. 15, 1–16. https://doi.org/10.1016/j.ecocom.2013.06.003.
Jamaly, R., Parent, S.-É., Parent, L.E., 2021. Fertilization and soil nutrients impact differentially cranberry yield and quality in Eastern Canada. Horticulturae 7, 191. https://doi.org/10.3390/horticulturae7070191.
Kganyago, M., Adjorlolo, C., Mhangara, P., 2022. Exploring transferable techniques to retrieve crop biophysical and biochemical variables using Sentinel-2 Data. Remote Sens. (Basel) 14, 3968. https://doi.org/10.3390/rs14163968.
Lawrence, L., Wood, D., Sheley, R., 2006. Mapping invasive plants using hyperspectral imagery and Breiman Cutler classifications (randomForest). Remote Sens. Environ. 100, 356–362. https://doi.org/10.1016/j.rse.2005.10.014.
Li, D., Cheng, T., Zhou, K., Zheng, H., Yao, X., Tian, Y., Zhu, Y., Cao, W., 2017. WREP: A wavelet-based technique for extracting the red edge position from reflectance spectra for estimating leaf and canopy chlorophyll contents of cereal crops. ISPRS J. Photogramm. Remote Sens. 129, 103–117. https://doi.org/10.1016/j.isprsjprs.2017.04.024.
Lincoln, N., Radovich, T., Acosta, K., Isele, E., Cho, A., 2019. Toward standardized leaf sampling for foliar nutrient analysis in Breadfruit. HortTechnology 29, 443–449. https://doi.org/10.21273/HORTTECH04358-19.
Liu, N., Chlus, A., Townsend, P.A., 2019. HyToolsPro: An open source package for pre-processing airborne hyperspectral images, in: 2019 Fall Meeting AGU. San Francisco, CA, pp. GC51E-1120.
Liu, N., Townsend, P.A., Naber, M.R., Bethke, P.C., Hills, W.B., Wang, Y., 2021. Hyperspectral imagery to monitor crop nutrient status within and across growing seasons. Remote Sens. Environ. 255, 112303 https://doi.org/10.1016/j.rse.2021.112303.
Mundorf, T., Wortmann, C., Shapiro, C., Paparozzi, E., 2015. Time of day effect on foliar nutrient concentrations in corn and soybean. J. Plant Nutr. 38, 2312–2325. https://doi.org/10.1080/01904167.2014.939760.
Mutanga, O., Skidmore, A.K., Kumar, L., Ferwerda, J., 2005. Estimating tropical pasture quality at canopy level using band depth analysis with continuum removal in the visible domain. Int. J. Remote Sens. 26, 1093–1108. https://doi.org/10.1080/01431160512331326738.
Pan, S.J., Yang, Q., 2010. A Survey on Transfer Learning. IEEE Trans. Knowl. Data Eng. 22, 1345–1359. https://doi.org/10.1109/TKDE.2009.191.
Pandey, P., Ge, Y., Stoerger, V., Schnable, J.C., 2017. High Throughput In vivo Analysis of Plant Leaf Chemical Properties Using Hyperspectral Imaging. Front. Plant Sci. 8 https://doi.org/10.3389/fpls.2017.01348.
Parent, L.E., Jamaly, R., Atucha, A., Jeanne Parent, E., Workmaster, B.A., Ziadi, N., Parent, S.-É., 2021. Current and next-year cranberry yields predicted from local features and carryover effects. PLoS One 16, e0250575. https://doi.org/10.1371/journal.pone.0250575.
Parent, L.E., Marchand, S., 2006. Response to Phosphorus of Cranberry on High Phosphorus Testing Acid Sandy Soils. Soil Sci. Soc. Am. J. 70, 1914–1921. https://doi.org/10.2136/sssaj2005.0194.
Pullanagari, R.R., Kereszturi, G., Yule, I.J., 2016. Mapping of macro and micro-nutrients of mixed pastures using airborne AisaFENIX hyperspectral imagery. ISPRS J. Photogramm. Remote Sens. 117, 1–10. https://doi.org/10.1016/j.isprsjprs.2016.03.010.
Pullanagari, R.R., Dehghan-Shoar, M., Yule, I.J., Bhatia, N., 2021. Field spectroscopy of canopy nitrogen concentration in temperate grasslands using a convolutional neural network. Remote Sens. Environ. 257, 112353 https://doi.org/10.1016/j.rse.2021.112353.
Queally, N., Ye, Z., Zheng, T., Chlus, A., Schneider, F., Pavlick, R.P., Townsend, P.A., 2022. FlexBRDF: A Flexible BRDF Correction for Grouped Processing of Airborne Imaging Spectroscopy Flightlines. J. Geophys. Res. Biogeosci. 127 https://doi.org/10.1029/2021JG006622.
Ramoelo, A., Skidmore, A.K., Cho, M.A., Mathieu, R., Heitkönig, I.M.A., Dudeni-Tlhone, N., Schlerf, M., Prins, H.H.T., 2013. Non-linear partial least square regression increases the estimation accuracy of grass nitrogen and phosphorus using in situ hyperspectral and environmental data. ISPRS J. Photogramm. Remote Sens. 82, 27–40. https://doi.org/10.1016/j.isprsjprs.2013.04.012.
Reich, P., 2012. Key canopy traits drive forest productivity. Proc Royal Soc B 279, 2128–2134. https://doi.org/10.1098/rspb.2011.2270.
Roper, T.R., 2006. The physiology of cranberry yield. University of Wisconsin- Madison Extension, Madison.
Roper, T.R., 2008. Cranberry production in Wisconsin. Madison.
Serbin, S.P., Singh, A., McNeil, B.E., Kingdon, C.C., Townsend, P.A., 2014. Spectroscopic determination of leaf morphological and biochemical traits for northern temperate and boreal tree species. Ecol. Appl. 24, 1651–1669. https://doi.org/10.1890/13-2110.1.
Settles, B., 2010. Active learning literature survey. Madison, Wisconsin, USA.
Singh, L., Mutanga, O., Mafongoya, P., Peerbhay, K., Crous, J., 2022. Hyperspectral remote sensing for foliar nutrient detection in forestry: A near-infrared perspective. Remote Sens Appl 25, 100676. https://doi.org/10.1016/j.rsase.2021.100676.
Song, X., Feng, W., He, L., Xu, D., Zhang, H.-Y., Li, X., Wang, Z.-J., Coburn, C.A., Wang, C.-Y., Guo, T.-C., 2016. Examining view angle effects on leaf N estimation in wheat using field reflectance spectroscopy. ISPRS J. Photogramm. Remote Sens. 122, 57–67. https://doi.org/10.1016/j.isprsjprs.2016.10.002.
United States Department of Agriculture, 2022. Wisconsin Ag News – Cranberries.
Upreti, D., Huang, W., Kong, W., Pascucci, S., Pignatti, S., Zhou, X., Ye, H., Casa, R., 2019. A comparison of hybrid machine learning algorithms for the retrieval of wheat biophysical variables from Sentinel-2. Remote Sens. 11, 481. https://doi.org/10.3390/rs11050481.
Van Cleemput, E., Vanierschot, L., Fernández-Castilla, B., Honnay, O., Somers, B., 2018. The functional characterization of grass- and shrubland ecosystems using hyperspectral remote sensing: trends, accuracy and moderating variables. Remote Sens. Environ. 209, 747–763. https://doi.org/10.1016/j.rse.2018.02.030.
Verrelst, J., Camps-Valls, G., Muñoz-Marí, J., Rivera, J.P., Veroustraete, F., Clevers, J.G.P.W., Moreno, J., 2015. Optical remote sensing and the retrieval of terrestrial vegetation bio-geophysical properties – A review. ISPRS J. Photogramm. Remote Sens. 108, 273–290. https://doi.org/10.1016/j.isprsjprs.2015.05.005.
Verrelst, J., Rivera, J.P., Gitelson, A., Delegido, J., Moreno, J., Camps-Valls, G., 2016. Spectral band selection for vegetation properties retrieval using Gaussian processes regression. Int. J. Appl. Earth Obs. Geoinf. 52, 554–567. https://doi.org/10.1016/j.jag.2016.07.016.
Verrelst, J., Berger, K., Rivera-Caicedo, J.P., 2021. Intelligent Sampling for Vegetation Nitrogen Mapping Based on Hybrid Machine Learning Algorithms. IEEE Geosci. Remote Sens. Lett. 18, 2038–2042. https://doi.org/10.1109/LGRS.2020.3014676.
Wan, L., Zhou, W., He, Y., Wanger, T.C., Cen, H., 2022. Combining transfer learning and hyperspectral reflectance analysis to assess leaf nitrogen concentration across different plant species datasets. Remote Sens. Environ. 269, 112826 https://doi.org/10.1016/j.rse.2021.112826.
Wang, Z., Townsend, P.A., Schweiger, A.K., Couture, J.J., Singh, A., Hobbie, S.E., Cavender-Bares, J., 2019. Mapping foliar functional traits and their uncertainties across three years in a grassland experiment. Remote Sens. Environ. 221, 405–416. https://doi.org/10.1016/j.rse.2018.11.016.
Wang, Z., Chlus, A., Geygan, R., Ye, Z., Zheng, T., Singh, A., Couture, J.J., Cavender-Bares, J., Kruger, E.L., Townsend, P.A., 2020. Foliar functional traits from imaging spectroscopy across biomes in eastern North America. New Phytol. 228, 494–511. https://doi.org/10.1111/nph.16711.
Wang, Z., Townsend, P.A., Kruger, E.L., 2022. Leaf spectroscopy reveals divergent inter- and intra-species foliar trait covariation and trait–environment relationships across NEON domains. New Phytol. 235, 923–938. https://doi.org/10.1111/nph.18204.
Watt, M.S., Pearse, G.D., Dash, J.P., Melia, N., Leonardo, E.M.C., 2019. Application of remote sensing technologies to identify impacts of nutritional deficiencies on forests. ISPRS J. Photogramm. Remote Sens. 149, 226–241. https://doi.org/10.1016/j.isprsjprs.2019.01.009.
Watt, M.S., Buddenbaum, H., Leonardo, E.M.C., Estarija, H.J.C., Bown, H.E., Gomez-Gallego, M., Hartley, R., Massam, P., Wright, L., Zarco-Tejada, P.J., 2020. Using hyperspectral plant traits linked to photosynthetic efficiency to assess N and P partition. ISPRS J. Photogramm. Remote Sens. 169, 406–420. https://doi.org/10.1016/j.isprsjprs.2020.09.006.
Wright, I.J., Reich, P.B., Westoby, M., Ackerly, D.D., Baruch, Z., Bongers, F., Cavender-Bares, J., Chapin, T., Cornelissen, J.H.C., Diemer, M., Flexas, J., Garnier, E., Groom, P.K., Gulias, J., Hikosaka, K., Lamont, B.B., Lee, T., Lee, W., Lusk, C., Midgley, J.J., Navas, M.-L., Niinemets, Ü., Oleksyn, J., Osada, N., Poorter, H., Poot, P., Prior, L., Pyankov, V.I., Roumet, C., Thomas, S.C., Tjoelker, M.G., Veneklaas, E.J., Villar, R., 2004. The worldwide leaf economics spectrum. Nature 428, 821–827. https://doi.org/10.1038/nature02403.
Xu, M., Liu, R., Chen, J.M., Shang, R., Liu, Y., Qi, L., Croft, H., Ju, W., Zhang, Y., He, Y., Qiu, F., Li, J., Lin, Q., 2022. Retrieving global leaf chlorophyll content from MERIS data using a neural network method. ISPRS J. Photogramm. Remote Sens. 192, 66–82. https://doi.org/10.1016/j.isprsjprs.2022.08.003.
Zhai, Y., Cui, L., Zhou, X., Gao, Y., Fei, T., Gao, W., 2013. Estimation of nitrogen, phosphorus, and potassium contents in the leaves of different plants using laboratory-based visible and near-infrared reflectance spectroscopy: comparison of partial least-square regression and support vector machine regression met. Int. J. Remote Sens. 34, 2502–2518. https://doi.org/10.1080/01431161.2012.746484.
Zhang, Y., Hui, J., Qin, Q., Sun, Y., Zhang, T., Sun, H., Li, M., 2021. Transfer-learning-based approach for leaf chlorophyll content estimation of winter wheat from hyperspectral data. Remote Sens. Environ. 267, 112724 https://doi.org/10.1016/j.rse.2021.112724.
Zhang, C., Kovacs, J., Wachowiak, M., Flores-Verdugo, F., 2013. Relationship between Hyperspectral Measurements and Mangrove Leaf Nitrogen Concentrations. Remote Sens. (Basel) 5, 891–908. https://doi.org/10.3390/rs5020891.